This article has been accepted for publication in a future issue of this journal, but has not been fully edited. Content may change prior to final publication. Citation information: DOI 10.1109/TIA.2018.2869098, IEEE Transactions on Industry Applications

Switched-Boost Action Based Multi-port Converter

Santanu K. Mishra, *Senior Member, IEEE*, Khirod Kumar Nayak, Mandeep Singh Rana, and Vimala Dharmarajan

Abstract: **Multi-output converters with single input source are currently studied as an alternative to conventional DC-DC topologies in order to improve power density in low power multi-load applications. The paper reviews three different ways in which a boost topology can be customized to supply multiple outputs. The first way uses a charge share approach using individual switches to distribute inductor energy to different capacitors. A second method of creating a multi-port converter combines two converters with similar front-end to generate two outputs using only one controlled switch. Using this method, a Boost converter can be combined with SEPIC, Cuk, and current source converter (CSC) topologies. A third method uses time-multiplexing of switches to produce two regulated ports and is referred to as Switched-boost action. This method uses relatively less number of switches and allows regulation and control of all the outputs. Practical utility of switched boost action based Multi-port Converter is reported in this work. This switched boost MPCis applied to a renewable power converter system to interface a solar panel, a battery, and home loads to produce a 12 V and a 48 V bus. The 12 V bus is interfaced to battery and capable of optimally charging the battery in CC-CV mode. The converter is demonstrated to operate with solar panel as it supplies a 12 V battery and a 48 V load bus. When the solar power is not available, the converter automatically goes into a mode in which the 12 V battery supplies the loads on the 48 V bus.**

I. Why Boost based Multi-port Converters?

Power converter with single input source and multiple outputs at different voltage levels is known as single input multiple output converter (SIMO). However, as in many applications, the same port works as both input and output (e.g., battery or grid interfaced ports), they are defined as multi-port converter (MPC) in this article, as depicted in Fig. 1. The outputs of this class of converter can either be higher or lower than the supply voltage depending on application. Some of the explored applications for these converters are on-chip supplies for consumer electronic devices [1-3], power supplies for consumer appliances[4-6], renewable energy integration in homes [7-8], and electric vehicles [9].MPCs can be isolated type or non-isolated type, as classified in Fig. 2. Isolated type MPC uses transformer with multiple secondary windings to interface with multiple loads. In this case, only one of the outputs is tightly-regulated and rests of the outputs are coupled through extra secondary windings. Non-isolated MPC have no galvanic isolation between different ports. However, depending on the number of inductors they can be further categorized into single inductor MPC (SI-MPC) or multiple inductor MPC (MI-MPC) [10], [11].

Manuscript received 14-APR-2018; revised 28-Jul-2018; accepted 10-Aug-2018. This work was supported by MHRD and Ministry of Power, Govt. of India under IMPRINT project F.No.3-18/2015-TS-I(Vol-III) – 7055. Santanu K. Mishra, Mandeep singh Rana and Vimala Dharmrajan are with the Department of Electrical Engineering at Indian Institute of Technology, Kanpur, India. Khirod Kumar Nayak is with ABB Global Industries Private Limited. (e mail: santanum@iitk.ac.in, khirod.bitu@gmail.com)

Color versions of one or more of the figures in this paper are available online at http://ieeexplore.ieee.org.

Digital Object Identifier:

Fig. 1. Block diagram of a Multi-port Converter.

Irrespective of the type of MPC, under ideal condition, power balance must be satisfied. Therefore, referring to Fig. 1, the power balance equation can be written as

$$V_1.I_1 + V_2.I_2 + V_3.I_3 = 0 \quad (1)$$

In the above equation, the current into all the ports is assumed to enter the positive terminal of the voltage at that port. For example, if port 1 is a source, ($V_1.I_1$) is positive and if port 2 is a load port, ($V_2.I_2$) is negative. It can be seen that as the output power increases, the input current also increases, if the input voltage is assumed constant. This criteria, forces the input current to be higher in boost topology due to smaller source voltage. Thus, achieving continuous conduction mode (CCM) operation in MPC is easier.

In this article, only non-isolated type MPCs are discussed. Normally, the passive and active components in a non-isolated DC-DC converter are traded while synthesizing different types of non-isolated MPCs. A converter with M controlled switches for M outputs leads to individually regulated output voltages. However, if a single switch is used to control multiple outputs, only one of the outputs can be fully regulated. In this case, the other outputs remain semi-regulated. Thus, the choice of MPCs is primarily a trade-off between requirement of regulating the outputs or simpler converter topology with less number of controlled switches and their control.

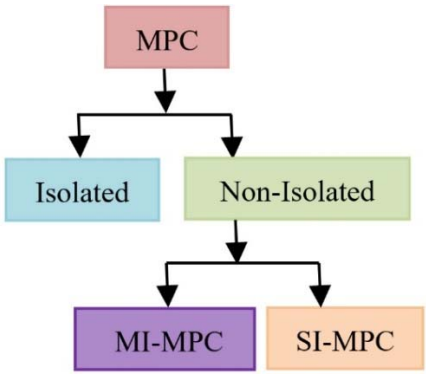

Fig. 2. Magnetics based Classification of different MPCs.

This article has been accepted for publication in a future issue of this journal, but has not been fully edited. Content may change prior to final publication. Citation information: DOI 10.1109/TIA.2018.2869098, IEEE Transactions on Industry Applications

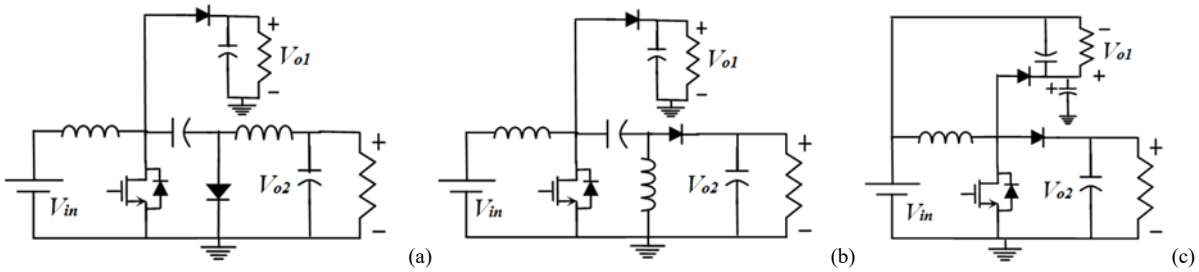

Fig. 3. Multi-output Boost topologies based on mix-match approach.(a) Boost and Cuk topology (b) Boost and SEPIC topology (c) Boost and current source topology.

In modern communication and computation devices, the ICs are powered with different voltage levels, which can be higher or lower than the supply input. Similarly, in renewable applications, boost converter is interfaced to a solar panel to enable a smaller input voltage to be used to obtain a higher DC link voltage. Reducing the input voltage in these applications, will lead to less number of series connected solar PV panels, and thus results in better power harvest under shaded condition. Thus, boost topology is an important topological choice to implement a MPC. It also has continuous DC input current as the source is directly interfaced with an inductor.

In this article, MPCs derived from boost topology are discussed. It is seen that there are primarily three class of boost topology based MPCs proposed in literature. The first one is based on charge share approach and it is discussed in SectionII. The second one is a class of MPC, which combines converter with same input stage to derive multiple outputs as will be discussed in Section III. It has limited regulation capability due to reduced active switch count. A third method to realize a MPC uses time multiplexing of switches of a modified boost topology to realize a three-port MPC. It is called switched boost MPC. This method is discussed in details in Section IV. A small renewable energy system based on switched boost MPC is also designed and validated.

II. MPC Based on Charge-Sharing Approach

This method of generating multiple outputs uses the concept of charge sharing [12]. The schematic of a two output boost topology using this approach is shown in Fig. 4(a). The inductor is charged using the switch S_B and in subsequent D' interval, rest of the switches S_1, S_2, etc. are turned on sequentially. Therefore, the charge is shared between output capacitors C_1, C_2, etc., respectively.

If S_1 is assumed to be a diode and the other switches are switched as per Fig. 4 (b), under continuous conduction mode (CCM), the output voltages can be derived using the following equation.

$$V_{dc1} = \frac{V_{in}}{1-\left(\frac{t_2+t_3}{t_s}\right)} V_{dc2} = \frac{t_2}{t_3}.\frac{R_2}{R_1}.V_{dc1} \qquad (1)$$

It can be observed that, even under CCM, the outputs are load dependent. Another important observation is that an output can be lower than the input voltage unlike a conventional boost converter.

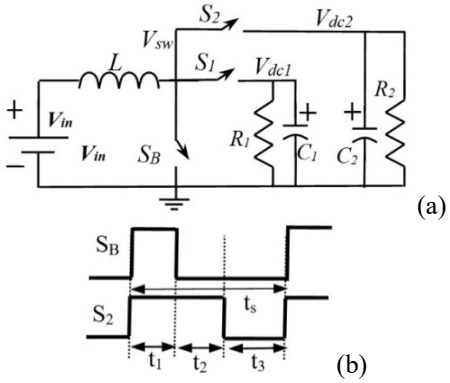

Fig.4. (a) SI-MPC converter with one supply and two outputs (b) Conventional switching scheme when S_1 is a diode.

This topology, its analysis and associated operational issues are extensively reported in literature [13-15]. As all the outputs are coupled to the same switch node in this class of MPCs, the outputs exhibit significant cross regulation. The dynamics of these converters are also poor. Several control approaches are reported in literature to improve cross-regulation and dynamic performance [16-19].

III. MPC Based on Mix-Match Approach

A method proposed in [20] combines various converters based on their front end. If the frontends of two converters are similar, then the rest of the converter parts are just combined to this front end to realize a MPC. For example, Fig. 3 shows three MPCs based on Boost converter. Fig. 3(a) shows a boost converter combined with Cuk converter, whereas Fig. 3(b) and (c) show the boost topology combined with SEPIC and current source converter (CSC).

In all the cases, the advantages are reduction in number of active switches. This leads to lower part count, reduction in driver circuits and simpler controller implementation. However, this topology has the disadvantage that both the outputs can't be regulated at the same time due to presence of one controllable switch.

IV. Switched-Boost Action

This method to synthesize a MPC was developed for low to medium power application and its principle of operation is summarized here. In this case, the idea is to keep the basic dynamic property of the converters intact and reduce the number of switches while realizing multiple outputs. The concept of time-multiplexing control for this approach is

This article has been accepted for publication in a future issue of this journal, but has not been fully edited. Content may change prior to final publication. Citation information: DOI 10.1109/TIA.2018.2869098, IEEE Transactions on Industry Applications

explained using Fig. 5(a) and (b). It is discussed in detail in [21-22]. To realize a MPC using this principle, the boost switch is replaced by a synchronous buck converter.

In this case, the boost interval is realized by turning on S_1 and S_2 at the same time. This will allow the boost inductor to charge. When both S_1 and S_2 are turned off, the inductor current routes to V_{out1}, similar to a conventional boost converter, which is referred to as zero interval. In this interval, the switch node (V_{SW1}) is clamped to V_{out1}.If S_1 is turned-on keeping S_2 off, the inductor current is routed to V_{out1} and V_{out2}. Note that when energy is getting transferred to $V_{out1}$and V_{out2}, the switch node voltage (V_{sw}) is clamped to V_{out1}. Thus, V_{out1} is the input voltage of the synchronous buck structure. In this interval, the power is routed to loads from the source, however the buck converter operates with an input of V_{out1}. Therefore, the circuit theory rule regarding two current sources in series (inductors $L_1$and L_2) is not violated. This is referred to as the buck interval in Fig. 5 (b).One major difference between this topology and the others described above is that in this case the buck converter is supplied by the input source, however its input voltage is decided by the output of the boost stage (V_{out1}). This principle is known as switched boost action [23]. By replacing a conventional diode with S_3, the converter structure is made capable of tri-directional power flow between V_{out1}, V_{out2}, and V_{in}. In order to demonstrate the tri-directional power capability of a Switched Boost MPC, it is used for renewable power distribution in a Solar powered DC Nanogrid with battery back-up.

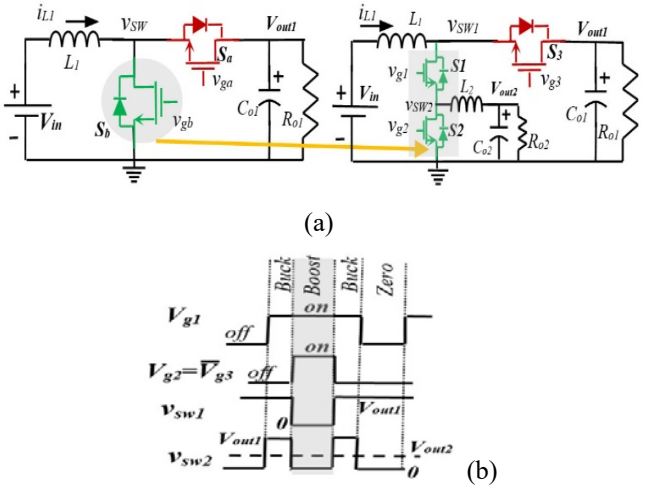

(a) (b)

Fig.5. (a) Switched Boost action to generate two outputs using a boost converter (b) Basic steady-state waveforms.

The advantages of a switched boost MPC topology are:
(i) Shoot through protection for buck topology
(ii) One less-switch and associated gate-driver and control circuit compared to individual buck and boost converter.
(iii) All the outputs are controllable
(iv) The dynamics of boost and buck stages are similar to original topology (analyzed in Fig. 11 and Fig. 15)
(v) Cross-regulation characteristics is very good.

V. Test-Case: An Application of Switched Boost MPC

A. Setup Overview

Switched Boost action based multi-output boost converter can find application in rural roof-top solar power distribution. As a test case, a 24 V input power supply with dual outputs is designed and verified in this section. A 48 V bus is interfaced to conventional home loads. A 12 V output is interfaced to a battery with optimal charging (CC-CV) functionalities. The power processing unit has two modes of operation:

(i) Mode A: 24 V input supply powers 48 V bus and charges the battery in CC-CV Mode (Fig. 6 (a))

(ii) Mode B: The input supply is cut-off (to simulate shading or night time conditions) and the 12 V battery powers the 48 V bus. (Fig. 6 (b))

The subsequent sub-sections explain the steady state operation and dynamic modeling of the multi-output topology in various modes of operation.

B. Mode A Operation

In this mode, the loads at 48V output bus and 12V output bus are supplied by the input solar power. The battery at the 12V output bus gets charged from the solar input. The converter in Mode-A operation has three different intervals. The steady-state waveforms during Mode-A operation is shown in Fig.7.

Interval I

The equivalent circuit for this interval is shown in Fig. 8 the switches S_1 and S_2 are turned on, simultaneously, to realize the boost operation of the converter. The current in inductor L_1 rises with a slope of m_1 ($=V_{in}/L_1$). The inductor current i_{L2} freewheels through switch $S_2$and has a slope of m_4 ($=V_{out2}/L_2$).During this interval, both the switch node voltages v_{sw1} and $v_{sw2}$are shorted to ground.

Interval II

In this interval, the switch S_2 is turned off and $S_3$is turned on and its diode is forward biased. The switch S_1also remains on. The duration of this interval is short in the applied switching

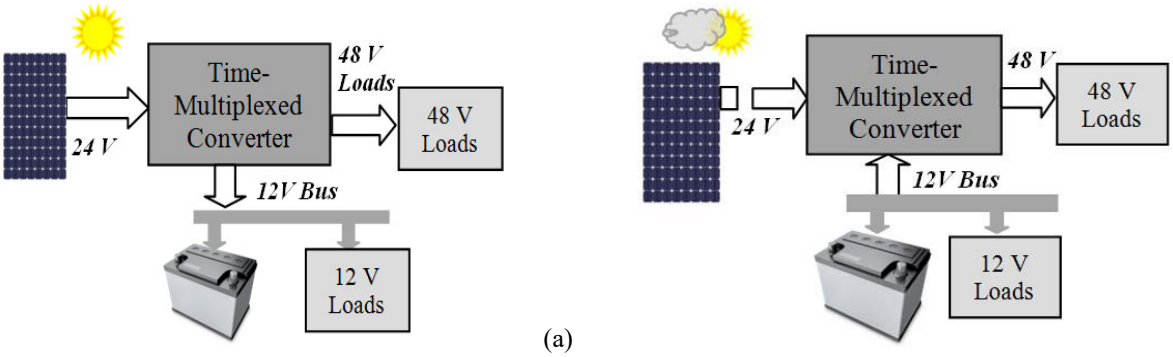

Fig. 6. System Configuration of a critical solar power supply. (a) Mode A: input source supplies both 12 V and 48 V loads (b) Mode B: 12 V battery supplies loads on 48 V.

This article has been accepted for publication in a future issue of this journal, but has not been fully edited. Content may change prior to final publication. Citation information: DOI 10.1109/TIA.2018.2869098, IEEE Transactions on Industry Applications

scheme, where the inductor current L_1 discharges with a slope of $m_2\left[=\frac{(V_{in}-V_{out1})}{L_1}\right]$ and L_2 starts charging with a slope of $m_3\left[\frac{(V_{out1}-V_{out2})}{L_2}\right]$ thus realizing buck operation with 12V output at battery end. Both the switch node voltages v_{sw1} and v_{sw2} are clamped to V_{out1}. It should also be noted that the input to the buck converter is fixed and it is equal to boost output voltage V_{out1}. The relevant equivalent circuit is given in Fig. 9.

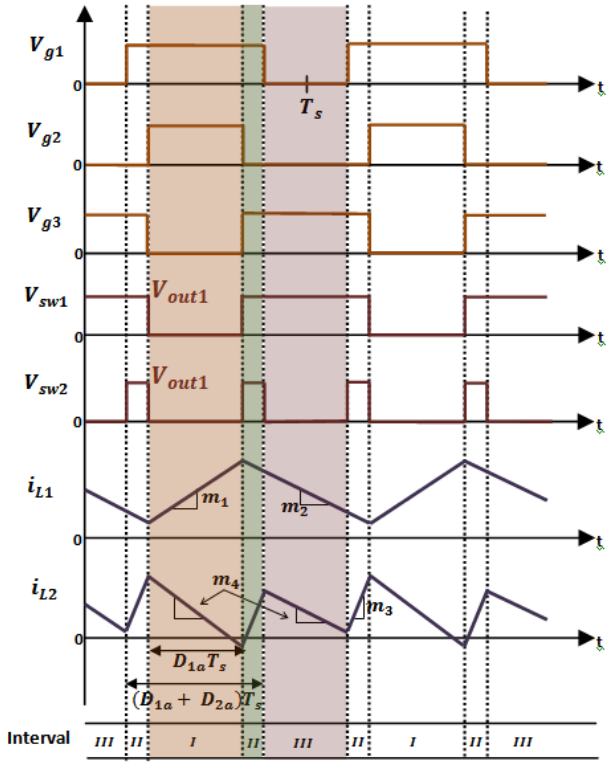

Fig.7. Steady state waveforms of the converter in Mode A.

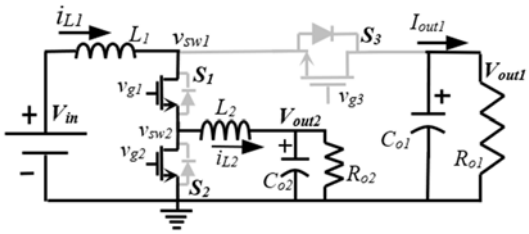

Fig. 8. Equivalent circuit for interval - I (Mode-A)

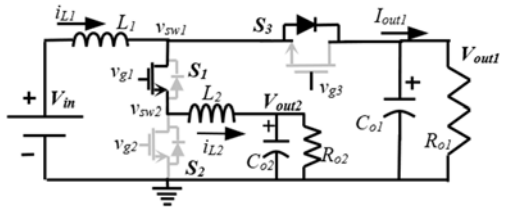

Fig. 9. Equivalent circuit for interval – II (Mode-A)

Interval III

In this interval, switch S_1 is turned off. This interval is similar to the freewheeling mode of conventional buck converter as shown in equivalent circuit given in Fig. 10. The switch S_3 or the antiparallel diode remains on. The inductor current i_{L2} freewheels through the body diode of $S_2$and has a slope of $m_4\left[=\frac{V_{out2}}{L_2}\right]$as in interval I.

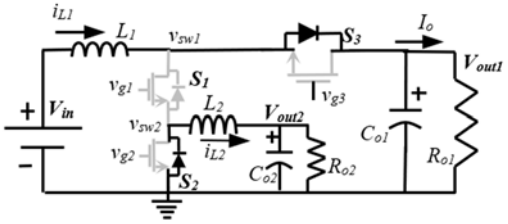

Fig. 10. Equivalent circuit for interval – III (Mode-A)

C. Modeling in Mode A

1) Steady-state Model

In this section, the steady-state voltage conversion ratio is derived for both the outputs. The waveforms are given in Fig. 6. Application of volt-sec balance across L_1 leads to

$$V_{in}.D_{1a} + (V_{in} - V_{out1}).(1 - D_{1a}) = 0$$

Here, D_{1a} is the fraction of time when both S_1 and S_2 are simultaneously turned-on. Thus, the boost output voltage is given by

$$V_{out1} = \frac{1}{1-D_{1a}}.V_{in} \quad (2)$$

In order to find an expression for V_{out2}, volt-sec balance is applied across the inductor L_2

$$-V_{out2}.D_{1a} + (V_{out1} - V_{out2}).D_{2a} + (-V_{out2}).(1 - D_{1a} - D_{2a}) = 0$$

Here D_{2a} is the fraction of interval when only $S_1$is turned-on. Thus, the steady state expression for V_{out2} is given by

$$V_{out2} = \frac{D_{2a}}{1-D_{1a}}.V_{in} \quad (3)$$

2) Dynamic Model

For circuit intervals described in mode A, the generalized state space equation can be written as

$$\dot{x}(t) = J * x(t) + K * u(t) \quad (4)$$

Here $\mathbf{x}(t)$ is vector containing all of the state variables that are inductor currents i_{L1}, i_{L2} and capacitor voltages v_{out1}, v_{out2}. u(t) is the independent input v_{in}.

$$\mathbf{x(t)} = [\mathrm{i_{L1}} \quad \mathrm{i_{L2}} \quad v_{out1} \quad v_{out2}]^T \text{and } \mathrm{u(t)} = v_{in} \quad (5)$$

During interval-1, (4) is written as

$$\dot{x}(t) = J_1 * x(t) + K_1 * u(t)$$

$$\text{Here, } \boldsymbol{J_1} = \begin{bmatrix} 0 & 0 & 0 & 0 \\ 0 & 0 & 0 & \frac{-1}{L_2} \\ 0 & 0 & \frac{-1}{C_{01}R_{01}} & 0 \\ 0 & \frac{1}{C_{02}} & 0 & \frac{-1}{C_{02}R_{02}} \end{bmatrix} \text{ and } \boldsymbol{K_1} = \begin{bmatrix} \frac{1}{L_1} \\ 0 \\ 0 \\ 0 \end{bmatrix}$$

During Interval-II, (4) is written as

$$\dot{x}(t) = J_2 * x(t) + K_2 * u(t)$$

$$\text{Here, } \boldsymbol{J_2} = \begin{bmatrix} 0 & 0 & \frac{-1}{L_1} & 0 \\ 0 & 0 & \frac{1}{L_2} & \frac{-1}{L_2} \\ \frac{1}{C_{01}} & \frac{-1}{C_{01}} & \frac{-1}{C_{01}R_{01}} & 0 \\ 0 & \frac{1}{C_{02}} & 0 & \frac{-1}{C_{02}R_{02}} \end{bmatrix} \text{ and } \boldsymbol{K_2} = \begin{bmatrix} \frac{1}{L_1} \\ 0 \\ 0 \\ 0 \end{bmatrix}$$

During interval-III, (4) is written as

This article has been accepted for publication in a future issue of this journal, but has not been fully edited. Content may change prior to final publication. Citation information: DOI 10.1109/TIA.2018.2869098, IEEE Transactions on Industry Applications

$$\dot{x}(t) = J_3 * x(t) + K_3 * u(t)$$

Here, $\boldsymbol{J_3} = \begin{bmatrix} 0 & 0 & \frac{-1}{L_1} & 0 \\ 0 & 0 & 0 & \frac{-1}{L_2} \\ \frac{1}{C_{01}} & 0 & \frac{-1}{C_{01}R_{01}} & 0 \\ 0 & \frac{1}{C_{02}} & 0 & \frac{-1}{C_{02}R_{02}} \end{bmatrix}$ and $\boldsymbol{K_3} = \begin{bmatrix} \frac{1}{L_1} \\ 0 \\ 0 \\ 0 \end{bmatrix}$

By applying state space averaging and perturbations in input $\hat{u}$ and control variables $\hat{d}_1$ and $\hat{d}_2$, the final state-space linearized equation can be obtained as

$$\hat{x} = [sI - J]^{-1} * [K * \hat{u}(s) + (J_1 - J_3) * X(s) * \hat{d}_{1a}(s) + (J_2 - J_3) * X(s) * \hat{d}_{2a}(s)] \quad (6)$$

Here

$$\boldsymbol{J} = \begin{bmatrix} 0 & 0 & \frac{-(1-D_{1a})}{L_1} & 0 \\ 0 & 0 & \frac{D_{2a}}{L_2} & \frac{-1}{L_2} \\ \frac{(1-D_{1a})}{C_{01}} & \frac{(-D_{2a})}{C_{01}} & \frac{-1}{C_{01}R_{01}} & 0 \\ 0 & \frac{1}{C_{02}} & 0 & \frac{-1}{C_{02}R_{02}} \end{bmatrix}, \boldsymbol{K} = \begin{bmatrix} \frac{1}{L_1} \\ 0 \\ 0 \\ 0 \end{bmatrix}, \hat{\boldsymbol{x}} = \begin{bmatrix} \hat{\imath}_{L1} \\ \hat{\imath}_{L2} \\ \hat{v}_{out1} \\ \hat{v}_{out2} \end{bmatrix}$$

The equation can be used to plot the control-to-output transfer function $\frac{\hat{v}_{out1}}{\hat{d}_{1a}}$. Fig. 11 compares the bode plot of a conventional boost topology with the boost stage transfer function $\frac{\hat{v}_{out1}}{\hat{d}_{1a}}$ of a switched boost MPC. The real-time simulation results from Pspice is also plotted to verify the accuracy of the analysis. As can be noted, as far as dynamics are concerned, the switched-boost MPC works very similar to a conventional boost converter which is a distinct advantage of this topology.

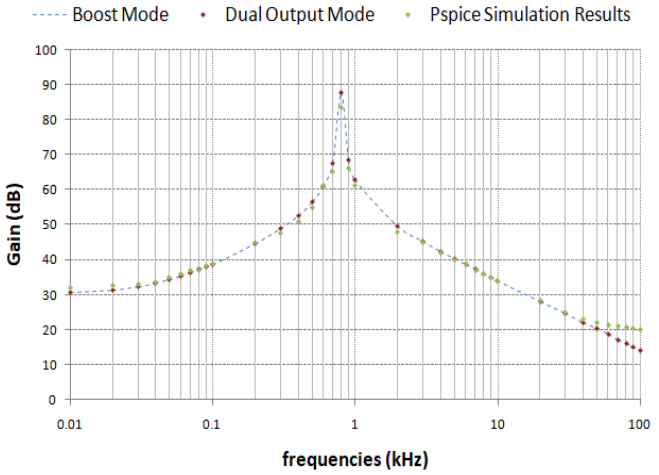

Fig. 11.Bode plot of Boost output verse control input ($\frac{\hat{v}_{out1}}{\hat{d}_{1a}}$) of a switched boost MPC during Mode A and its comparison to a conventional boost topology considering parameters mentioned in caption of Fig. 20.

D. Mode B Operation

In Mode B, the solar input is absent. The 12V battery supplies the loads on 12 V and 48 V bus. Thus, the gate pulses are modified to achieve boost operation from 12V battery as input to 48V output bus. The PWM signal to S_1 is removed in this mode. The steady state waveforms of the converter during mode B operation are given in Fig.12.There are two intervals in a switching cycle.

Interval I

At the start of this interval, switch S_2 is turned on. The inductor i_{L2} is charged with a slope of $m_5\left[=\frac{V_{out2}}{L_2}.\right]$. The switch S_3 is off. This interval is similar to boost operation with S_2 being on and L_2 is charged to input voltage. The equivalent circuit of this interval is given in Fig.13.

Interval II

The switch S_2 is turned off and S_3 is turned on at the start of this interval. The inductor L_2 starts delivering energy to 48V bus with a decreasing slope of $m_6\left[=\frac{(V_{out1}-V_{out2})}{L_2}\right]$. The equivalent circuit of this interval is given in Fig.14. It should be noted that under steady state the voltage across C_{in} is V_{out1}, and therefore, the current through L_1 is zero.

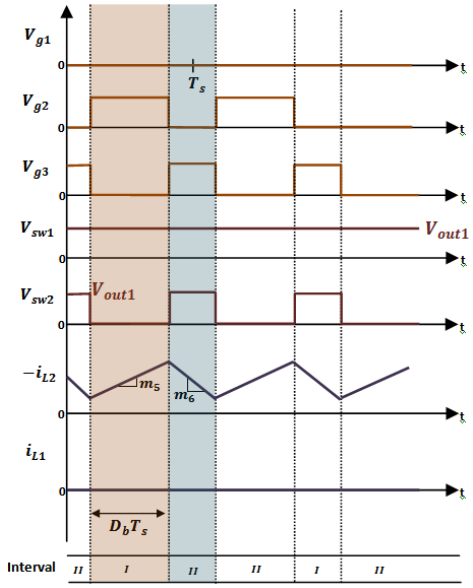

Fig.12. Steady state waveforms of the converter in Mode B.

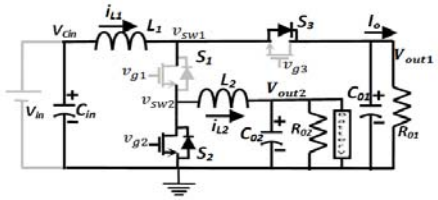

Fig.13. Equivalent circuit for interval - I (Mode-B)

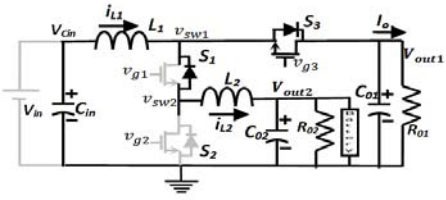

Fig.14. Equivalent circuit for interval - II (Mode-B)

E. Modeling in Mode B

1) Steady-state Model

In this section, the steady-state voltage conversion ratio is derived for output voltage V_{out1}. Application of volt-sec balance across L_2 leads to

$$-V_{out2}.D_bT_s + (V_{out1} - V_{out2}).D'_bT_s = 0$$

This article has been accepted for publication in a future issue of this journal, but has not been fully edited. Content may change prior to final publication. Citation information: DOI 10.1109/TIA.2018.2869098, IEEE Transactions on Industry Applications

Here, D_b is the fraction of time for which time S_2 is turned-on compared to time Period of switching. Thus, the boost output voltage is given by

$$\frac{V_{out1}}{V_{out2}} = \frac{V_{out1}}{V_{battery}} = \frac{1}{1-D_b} \quad (6)$$

2) Dynamic Model

For circuit intervals described in mode B, the generalize state space equation can be written as

$$\dot{x}(t) = P * x(t) + Q * u(t) \quad (7)$$

Here **x**(t) is vector containing all of the state variables that are inductor currents i_{L1}, i_{L2} and capacitor voltages v_{out1}, v_{out2}, v_{in}. $u(t)$ is the independent input E.

$$x(t) = [i_{L1} \quad i_{L2} \quad v_{out1} \quad v_{out2} \quad v_{in}]^T \text{ and } u(t) = E \quad (8)$$

During interval-1, (7) is written as

$$\dot{x}(t) = P_1 * x(t) + Q_1 * u(t)$$

$$\boldsymbol{P_1} = \begin{bmatrix} 0 & 0 & \frac{-1}{L_1} & 0 & \frac{1}{L_1} \\ 0 & 0 & 0 & \frac{-1}{L_2} & 0 \\ \frac{1}{C_{01}} & 0 & \frac{-1}{C_{01}R_{01}} & 0 & 0 \\ 0 & \frac{1}{C_{02}} & 0 & \frac{-(R_{02}+R_B)}{C_{02}R_{02}R_B} & 0 \\ \frac{-1}{C_{in}} & 0 & 0 & 0 & 0 \end{bmatrix}, \; Q_1 = \begin{bmatrix} 0 \\ 0 \\ 0 \\ \frac{1}{C_{02}R_B} \\ 0 \end{bmatrix}$$

During Interval-II, (7) is written as

$$\dot{x}(t) = P_2 * x(t) + Q_2 * u(t)$$

Here, $P_2 = \begin{bmatrix} 0 & 0 & \frac{-1}{L_1} & 0 & \frac{1}{L_1} \\ 0 & 0 & \frac{1}{L_2} & \frac{-1}{L_2} & 0 \\ \frac{1}{C_{01}} & \frac{-1}{C_{01}} & \frac{-1}{C_{01}R_{01}} & 0 & 0 \\ 0 & \frac{1}{C_{02}} & 0 & \frac{-(R_{02}+R_B)}{C_{02}R_{02}R_B} & 0 \\ \frac{-1}{C_{in}} & 0 & 0 & 0 & 0 \end{bmatrix}, Q_2 = \begin{bmatrix} 0 \\ 0 \\ 0 \\ \frac{1}{C_{02}R_B} \\ 0 \end{bmatrix}$

By applying state space averaging to these intervals for small perturbations in input û and control variable $\hat{d}_b$, the final state-space linearized equation can be obtained as

$$\hat{x} = [sI - P]^{-1} * [Q * \hat{u}(s) + (P_1 - P_2) * X(s) * \hat{d}_b(s)] \quad (9)$$

Here, $P = \begin{bmatrix} 0 & 0 & \frac{-1}{L_1} & 0 & \frac{1}{L_1} \\ 0 & 0 & \frac{(1-D_b)}{L_2} & \frac{-1}{L_2} & 0 \\ \frac{1}{C_{01}} & \frac{-(1-D_b)}{C_{01}} & \frac{-1}{C_{01}R_{01}} & 0 & 0 \\ 0 & \frac{1}{C_{02}} & 0 & \frac{-(R_{02}+R_B)}{C_{02}R_{02}R_B} & 0 \\ \frac{-1}{C_{in}} & 0 & 0 & 0 & 0 \end{bmatrix}, Q = \begin{bmatrix} 0 \\ 0 \\ 0 \\ \frac{1}{C_{02}R_B} \\ 0 \end{bmatrix}$

The equation can be used to plot the control-to-output transfer function $\frac{\hat{v}_{out1}}{\hat{d}_b}$.

Fig. 15 compares the bode plot of a boost topology with the boost stage transfer function $\frac{\hat{v}_{out1}}{\hat{d}_b}$ neglecting C_{in} and L_1 of a switched boost MPC for mode B. The real-time simulation results from Pspice is also plotted to verify the accuracy of the analysis.

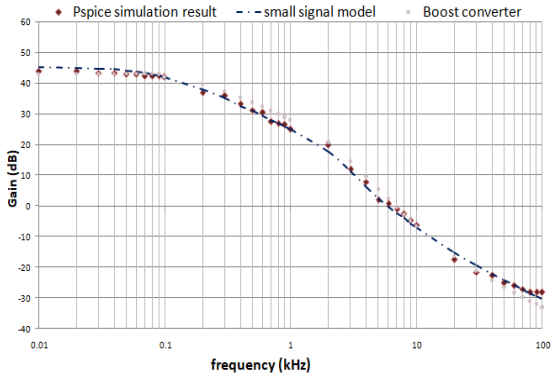

Fig. 15. Bode plot of $\frac{\hat{v}_{out1}}{\hat{d}_b}$during Mode B operation and its comparison to a conventional boost topology (neglecting C_{in} and L_1) considering parameters mentioned in Fig. 20.

F. Optimal Battery Charging Control

In order to review CC-CV mode of charging, Fig. 16. (a) shows a typical experimental optimal charging of a battery, where it is charged with a constant current when its state-of-charge (SOC) is low and charged with a constant voltage when its SOC is near 100 %. A typical control circuit to implement optimal charging is shown in Fig. 16(b) and is discussed in [24-25].

The controller has an inner current loop and an outer voltage loop. The voltage compensator output is clamped using a Zener diode. When battery SOC is low (V_{bat}<V_{ref}), the output of the voltage compensator is clamped to V_z; thus, making the current controller reference fixed at V_z. This is shown in Fig. 17 (a). Therefore, a constant I_L(=V_z/k_c)is supplied by the converter. However, when the battery SOC is close to V_{ref}, the voltage loop works like a conventional voltage mode controller and I_{crg} is no longer clamped to V_z. The controller during this mode of operation is shown in Fig. 17 (b).This scheme will be used to implement the roof-top solar power system explained below.

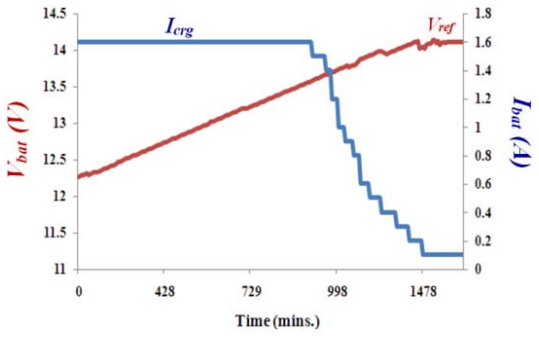

(a)

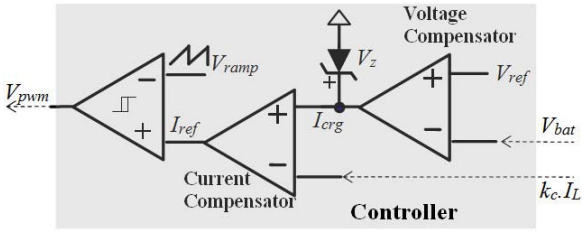

(b)

Fig. 16. (a) Optimal battery charging characteristic (b) control circuit for automatic optimal charging of a battery.

This article has been accepted for publication in a future issue of this journal, but has not been fully edited. Content may change prior to final publication. Citation information: DOI 10.1109/TIA.2018.2869098, IEEE Transactions on Industry Applications

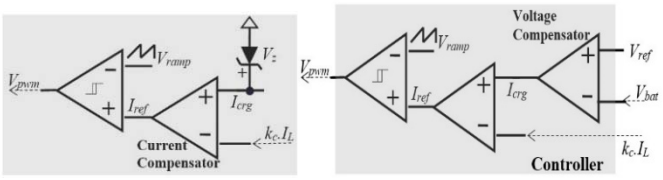

(a) (b)

Fig. 17. Controller architecture during different battery state of charge. (a) as a constant current controller (b) working as a voltage source controller.

G. *Controller operation in different modes*

The power stage works as discussed in the prior sections. This section gives insight into control scheme of the converter in two different operation modes. Both the 48V and 12V outputs are regulated using analog controllers. The boost output (V_{out1}) is regulated to 48 V using a voltage controller (control #1). The step-down output (V_{out2}) is interfaced to a battery and is controlled by control #2. Its control is implemented using an optimal battery charging control as given in Fig. 16 (b). Both the controller outputs are processed using analog PWM controllers. Here PWM for switch S_1controls the battery output and PWM for switch S_2 regulates the 48 V output. A mode selection circuit toggles the control between Mode A and Mode B based on input voltage magnitude.

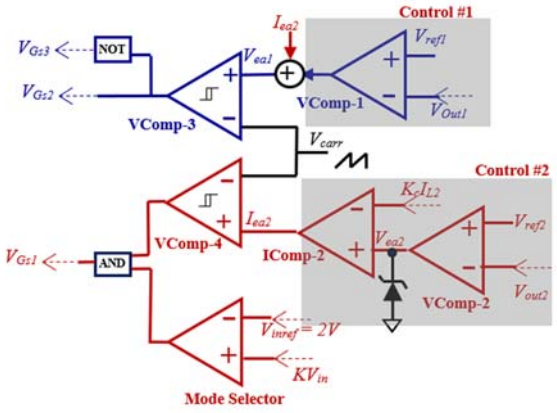

Fig.18.Controller architecture in Mode-A.

Mode A: During Mode A of operation, the input source (V_{in}) supplies both the outputs. The control circuit in Mode A is given in Fig.18. The basic idea is to regulate V_{out1} using control #1 (drawn in blue) and optimally charge battery on V_{out2} using control #2 (drawn in red) in Fig. 18. Once the battery is fully charged, the control #2 in Fig. 18 automatically reverts to voltage mode control and regulate the output voltage, as was explained in Fig. 17 (b).The start-up and steady state operation for this mode of operation is shown in Fig. 19(a) and (b). As soon as the start-up is initiated at t_1, the battery and the input source start charging the output voltage and supply the load at V_{out1}. At t_2, the input current is sufficient to supply the both the output loads. Therefore, the battery current reverses direction and starts charging and reaches a steady state at instant t_3. After t_3, both the loads are steadily supplied by the input source.

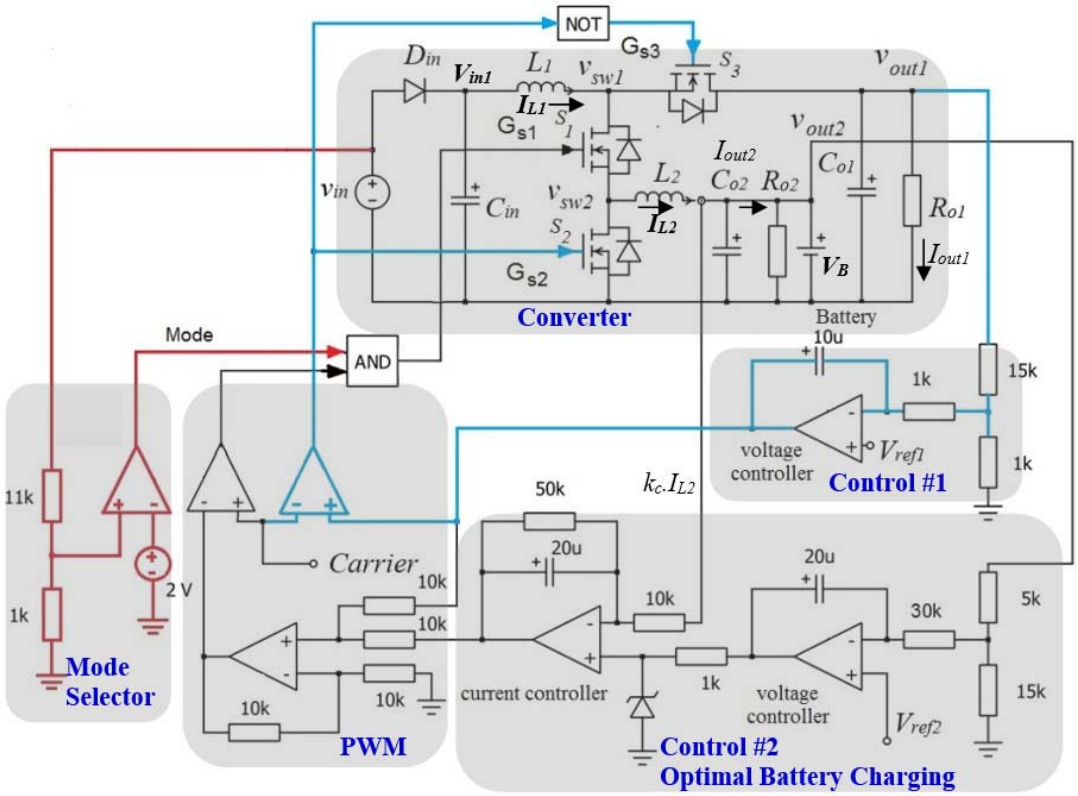

Fig. 20 Schematic of time-multiplexed converter and control. Design parameters for prototype: L_1=15 uH, L_2=10 uH, C_{o1}=660 uF, C_{o2}=440 uF, C_{in}=200 uF, V_B=12 V, Load is variable up to maximum 200 W.

This article has been accepted for publication in a future issue of this journal, but has not been fully edited. Content may change prior to final publication. Citation information: DOI 10.1109/TIA.2018.2869098, IEEE Transactions on Industry Applications

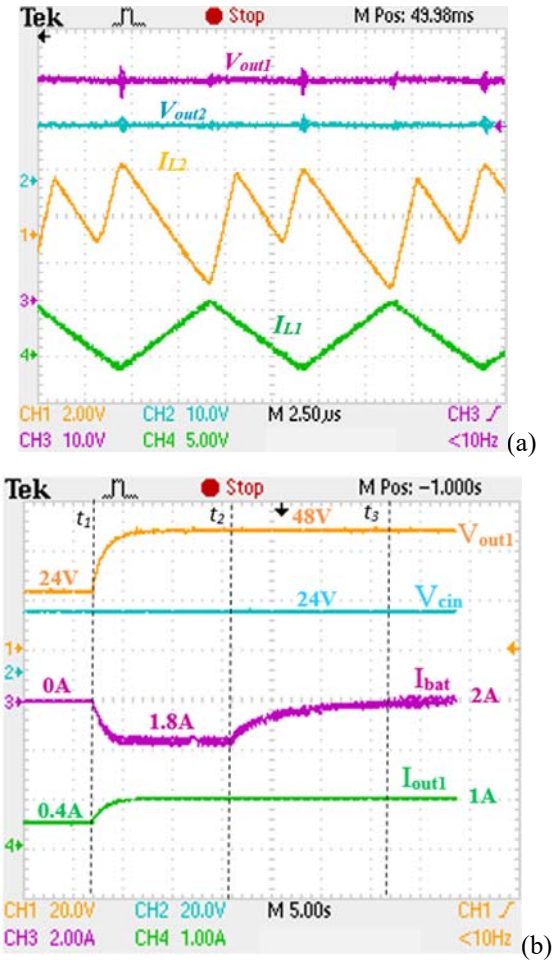

Fig. 19. (a) Switching waveform in Mode A under steady-state (b) Start-up and steady state behavior in Mode A with 12 V

Mode B: The control circuit in mode B is shown in Fig. 21.As the battery is the source in this mode, the control only regulates the V_{out1} at 48 V. This start up is shown in Fig. 22.Between t_1 to t_2, the battery current (I_{out2}) charges the 48 V output. After t_2, it reaches a steady state. Note I_{out1} is smaller than I_{bat} because of power balance and it is at 48 V level.

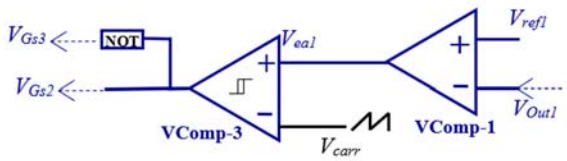

Fig.21. controller operation in Mode-B.

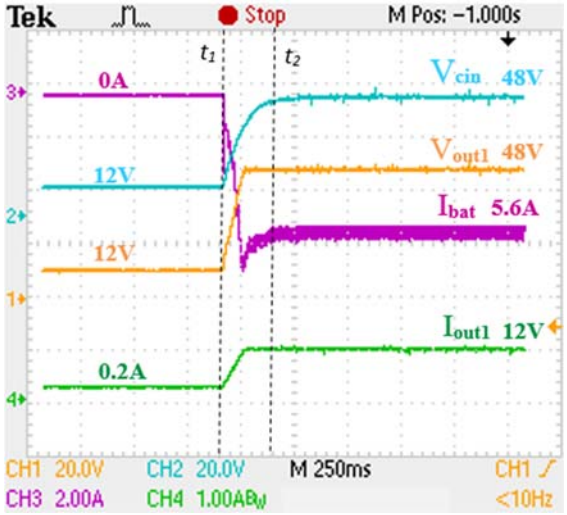

Fig. 22. Start-up and steady-state behaviour in Mode B

Transition between Mode A and Mode B: The transition from Mode A to Mode B, as shown in Fig. 23 (a) is enforced by starting up the converter in Mode A and reducing the input source voltage. The mode selector switches the converter such that the battery supplies the 48 V load. Before t_1, the input source is charging the battery and supplying the 48 V bus as is evident from the direction of I_{L2}. At t_1, the transition from Mode A to Mode B is initiated by reducing the supply voltage. At time instant t_2, the controller responds to the transition to Mode B. Therefore, the current through L_2 ($=I_{L2}$) changes direction. The battery internal resistance at this instant decides the drop observed in V_{out2}. During the transition, there is also a transient drop in the 48 V bus. The drop is dependent on the speed of the feedback loop and the storage capacitor present on the bus. After t_3, the transition to Mode B is complete and the output voltages are regulated. Fig. 23 (b) shows the battery current behavior (Shaded portion) when the 48V (V_{out1}) output load was removed. It can be seen that the battery being charged for few secs with the V_{cin} voltage. In this mode, the load on 12 V bus are the only one supported by the source.

Step load change in Mode A: The response of the converter to a step change in load on one output terminal on other outputs is verified in this sub-section. Fig. 24 shows the response of the converter outputs to a 1 A load step-up at the 48 V terminal while keeping the load at the 12 V terminal constant. It is observed that there is negligible response on the outputs to this load transient.

The transient response of the converter to a load step-up and step-down at the 12 V terminal with the load at 48 V constant is shown in Fig. 25. The responses prove excellent cross regulation characteristics of the converter during normal operation.

This article has been accepted for publication in a future issue of this journal, but has not been fully edited. Content may change prior to final publication. Citation information: DOI 10.1109/TIA.2018.2869098, IEEE Transactions on Industry Applications

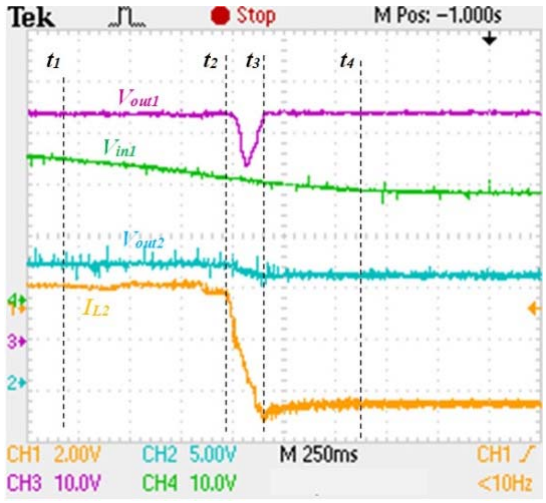

(a)

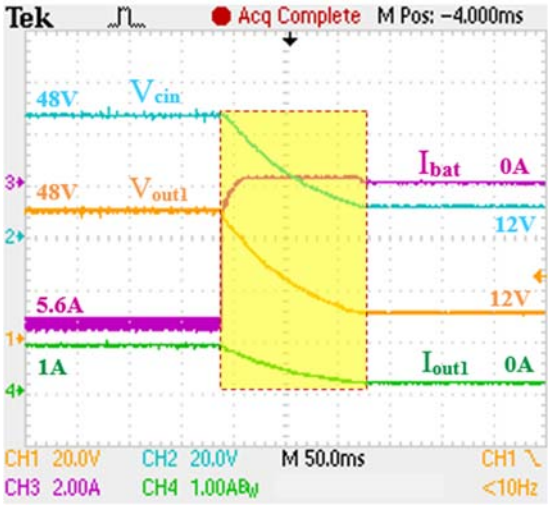

(b)

Fig. 23. (a) Transition between Mode A (with 12 V battery in CC mode of charging) to Mode B. (b) Battery current behaviour (Shaded portion) when the 48V output (Vout1) regulation is turned off.

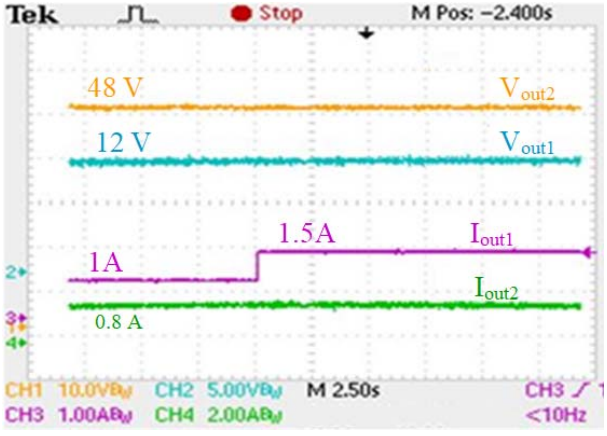

Fig. 24. Response of the converter to a 1 A step-up load change at the 48 V terminal.

Step load change in Mode B: The response of the converter to a step change in load on step up output terminal is verified in this sub-section. Fig. 26. Shows the response of the converter outputs to a 0.5 A load step at the 48 V terminal while keeping the load at the 12 V terminal constant. It is observed that there is negligible impact on the voltage outputs due this load transient.

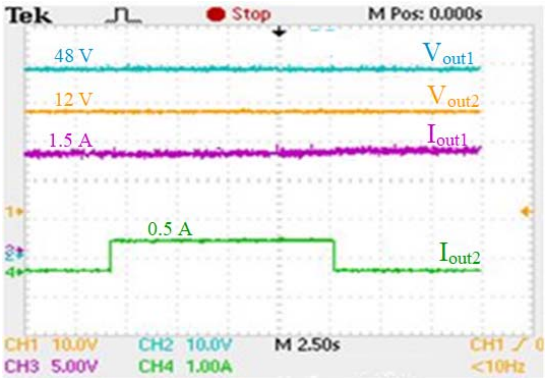

Fig. 25. Response of the converter to a load steps at the 12 V terminal.

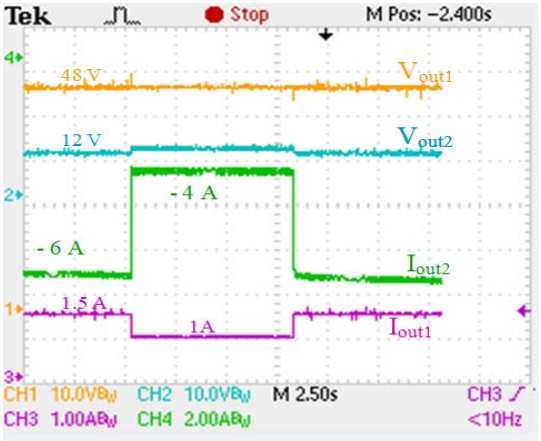

Fig. 26. Step load change at 48 V output terminal with Mode B operation.

VI. References

[1] Rong-Jong Wai, and Jun-Jie Liaw"High-Efficiency-Isolated Single-InputMultiple-Output Bidirectional Converter," in *IEEE Transactions On Power Electronics*, Vol. 30, No. 9, September 2015, pp. 4914-4930.

[2] P. Patra, A. Patra, and N. Mishra, "Single-Inductor Multiple-Output Switcher WithSimultaneous Buck, Boost, and Inverted Outputs," in *IEEE Transactions On Power Electronics*, Vol. 27, No. 4, April 2012, pp. 1936-1951.

[3] D. Ma, W.-H. Ki, C. Y. Tsui, and P. K. T. Mok, "Single-inductor multiple-output switching converters with time-multiplexing control in discontinuous conduction mode," *IEEE J. Solid-State Circuits*, vol. 38, pp. 89–100, Jan. 2003.

[4] Hyun-Chang Kim, Chang Soo Yoon, Deog-Kyoon Jeong, and Jaeha Kim, "A Single-Inductor, Multiple-Channel Current-Balancing LED Driver for Display Backlight Applications," in *IEEE Transactions On Industry Applications*, Vol. 50, No. 6, Nov. 2014, pp. 4077-4081.

[5] Kumar Modepalli and Leila Parsa, "A Scalable N-Color LED Driver Using Single Inductor Multiple Current Output Topology," in *IEEE Transactions On Power Electronics*, Vol. 31, No. 5, May 2016, pp. 3773-3783.

[6] Rajiv Damodaran Prabha and Gabriel A. Rincón-Mora, "Battery-assisted and Photovoltaic-sourced Switched-inductor CMOS Harvesting Charger–Supply," in *IEEE International Symposium on Circuits and Systems (ISCAS2013)*, pp. 253-256.

[7] H. Shao, X. Li, C. Y. Tsui, and W. H. Ki, "A novel single-inductor dual-input dual-output DC-DC converter with PWM control for solar energy harvesting system," *IEEE Trans. VLSI Syst.*, vol. 22, no. 8, pp. 1693- 1704, Aug. 2014.

[8] Y. Qian, H. Zhang, Y. Chen, Y. Qin, D. Lu, and Z. Hong, "A SIDIDO DC–DC converter with dual-mode and programmable-capacitor-array MPPT control for thermoelectric energy harvesting," in *IEEE Trans. Circuits and Systems II: Express Briefs*, vol. 64, no. 8, pp. 952-956, Aug. 2017.

[9] Nahavandi A, Hagh M T, Sharifian M B B, et al. "A Non-isolated multi-input multioutput DC–DC boost converter for electric vehicle applications," *IEEE Trans. Power Electron.*, vol. 30, no. 4, pp. 1818- 1835, 2015.

[10] Benfei Wang, Xinan Zhang, *Member,* Jian Ye, Hoay Beng Gooi, "Deadbeat Control for Single-Inductor Multiple-Input Multiple-Output DC-DC Converter," in*IEEE Trans. Power Electron.*, early access, 2018.
[11] T. Kerekes, M. Liserre, R. Teodorescu, C. Klumpner, and M. Sumner, "Evaluation of three-phase transformer-less photovoltaic inverter topologies," in *IEEE Trans. Power Electron.*, vol. 24, no. 9, pp. 2202–2211, Sep. 2009.
[12] Dongsheng Ma, Wing-Hung Ki, and Chi-Ying Tsui, "A Pseudo-CCM/DCM SIMO Switching Converter with Freewheel Switching," in *IEEE Journal on Solid-state Circuits*, Vol. 38, No. 6, pp. 1007-1014, June 2003.
[13] Young-Jin Moon, Yong-Seong Roh, Jung-Chul Gong, and Changsik Yoo, "Load-Independent Current Control Technique of a Single-Inductor Multiple-Output Switching DC–DC converter," in *IEEE Trans. Circuits and Systems II: Express Briefs*, vol. 59, no. 1, pp. 50-54, Jan. 2012.
[14] H. Behjati and A. Davoudi, "A multiple input multiple output dc–dc converter," *IEEE Trans. Ind. Appl*., vol. 49, no. 3, pp. 1464–1479, May 2013.
[15] Xiaocheng Jingand Philip K. T. Mok, "Power Loss and Switching Noise Reduction Techniques for Single-Inductor Multiple-Output Regulator," in *IEEE Trans. Circuits and Systems I*, vol. 60, no. 10, pp. 2788-2797, Oct 2013.
[16] Pradipta Patra, Jyotirmoy Ghosh, and Amit Patra, "Control Scheme for Reduced Cross-Regulation in Single-Inductor Multiple-Output DC–DC Converters," in *IEEE Trans. Ind. Electron.*, vol. 60, no. 11, pp. 5095-5103, Nov. 2013.
[17] C. N. Onwuchekwa and A. Kwasinski, "A modified-time-sharing switching technique for multiple-input dc–dc converters," IEEE Trans. Power Electron., vol. 27, no. 11, pp. 4492–4502, Nov. 2012.
[18] Ming-Hsin Huang and Ke-Horng Chen, "Single-Inductor Multi-Output (SIMO) DC-DC Converters with High Light-Load Efficiency and Minimized Cross-Regulation for Portable Devices," in *IEEE Journal on Solid-state Circuits*, Vol. 44, No. 4, pp. 1099-1111, April 2009.
[19] Benfei Wang, Liang Xian, Venkata Kanamarlapudi, et. al., "A Digital Method of Power-Sharing and Cross-Regulation Suppression for Single-Inductor Multiple-Input Multiple-Output DC–DC Converter," in *IEEE Trans. Ind. Electron.*, vol. 64, no. 4, pp. 2836-2847, April 2017.
[20] Maria Bella Ferrera Prieto, Salvador Pérez Litrán, Eladio Durán Aranda, And Juan Manuel Enrique Gómez, "New Single Input, Multiple Output Converter Topologies," in *IEEE Industrial Electronics Magazine*, June 2016, pp. 6-20.
[21] Santanu Mishra and Olive Ray, "Advances in nanogrid technology and its integration into rural electrification in India," in Proc. *IEEE IPEC-ECCE Asia*, Hiroshima, Japan, May 2014.
[22] Olive Ray, Anil Prasad, Santanu Mishra, and A. Joshi, "Integrated dual output converter," in *IEEE Trans. Ind. Electron.*, vol. 62, no. 1, pp. 371-382, Jan 2015.
[23] Olive Ray and Santanu Mishra, "Switched-boost action: a phenomenon for achieving time-division-multiplexed multi-port power transfer for nanogrid applications," in Sadhana, Vol. 42, No. 8, pp. 1227–1238, August 2017.
[24] Rajeev Singh and Santanu Mishra, "A magnetically coupled feedback-clamped optimal bi-directional battery charger," *IEEE Trans. Ind. Electron.*, vol. 60, no. 2, pp. 422–432, Feb. 2013.
[25] Santanu K. Mishra and Khirod Nayak, "Boost Topology Based Multi-Output Converters," in IEEE Industry Applications Society Annual Meeting, 2017, Cincinnati, OH.

Santanu K. Mishra (S'00-M'04-SM'12) received a B.Tech. degree in Electrical Engineering from the College of Engineering and Technology, Bhubaneswar, India, in 1998, an M.Tech. degree in Energy Systems Engineering from Indian Institute of Technology, Chennai, India, in 2000, and the Ph.D. degree from the Department of Electrical and Computer Engineering, University of Florida, Gainesville, FL, USA, in 2006.

He worked as a senior application engineer with the International Rectifier Corporation in Rhode Island, USA, from 2004 to 2008. Currently, he is a Professor at the Indian Institute of Technology, Kanpur, India. He was a visiting professor at Center for Power Electronics Systems (CPES) at Virginia Tech. during fall of 2017. His research interests include power converter design, implementation, control, and applications in rural scenario. He serves as an associate editor of several journals including IEEE Transactions on Industry Applications, IEEE Transactions on Power Electronics, IEEE Consumer Electronics Magazine, and IET Power Electronics.

Khirod Kumar Nayak, received his B-Tech degree in Electrical Engineering in 2009 from the Biju Patnaik University of Technology, Bhubaneswar and the M-Tech degree in Electrical Engineering from the Indian Institute of Technology Kanpur in 2016.

He is currently working as a R&D engineer in ABB Global Industries Private Limited in Chennai. His research interests include power converter design and control.

Mandeep Singh Rana, received a B.Tech. degree in Electrical Engineering from the National Institute of Technology, Bhopal, India, in 2013. He is currently pursuing his M.Tech. degree in Power Engineering from the Department of Electrical Engineering, Indian Institute of Technology, Kanpur, India. His research interests include power converter design and control.

Ms. Vimala Dharmarajan, received her B.E. degree in Electrical and Electronics Engineering from National Engineering College, Tamil Nadu. She received her MASc degree in Power Electronics in Electrical Engineering from the University of Victoria, Canada.

She is currently working as Project Engineer in the Department of Electrical Engineering at IIT Kanpur. Her research interests include power converter design and control.